CHAPTER 20

Magnetic Resonance in the Assessment of Tissue Engineered Cartilage

MRIGNAYANI KOTECHA*[a], ZIYING YIN[a] AND RICHARD L. MAGIN[a]

[a]Department of Bioengineering, University of Illinois at Chicago, 835, S. Wolcott Avenue, Chicago, IL 60612, USA
*E-mail: mkotecha@uic.edu

20.1 Introduction

According to the Centers for Disease Control and Prevention report on *Arthritis and Quality of Life 2015*, arthritis is one of the most common chronic conditions in American adults, afflicting approximately 1 in 5 people.[1] Arthritis is caused by damaged or diseased articular cartilage in synovial joints, such as the knee, ankle, hip, shoulder, or wrist. Cartilage enables smooth frictionless moving of these joints because of its special viscoelastic biomechanical properties. This ability is impaired when the tissue is damaged. Other than arthritis, conditions such as trauma, sports injury, or developmental issues can also cause damage to articular cartilage. The onset of cartilage damage results in ever-increasing pain and discomfort affecting the quality of life and ability to work.

New Developments in NMR No. 8
Biophysics and Biochemistry of Cartilage by NMR and MRI
Edited by Yang Xia and Konstantin I. Momot

Published by the Royal Society of Chemistry, www.rsc.org

Articular cartilage is an avascular, alymphatic, and aneural tissue with limited ability to repair and maintain itself in adults. At present, there is no cure for cartilage damage. It is generally managed using physical therapy, lifestyle changes, and analgesics. The limited self-healing capabilities of cartilage often result in surgical interventions to provide long-term healing to partial and full defect cartilage lesion sites. Over the years, many types of treatments have evolved to treat cartilage damage. These include bone-marrow stimulation, autologous chondrocyte implantation, and the osteochondral autograft transfer system.[2,3] Unfortunately, none of the available treatments have the potential to regenerate the biological composition and biomechanical properties of native cartilage, thereby providing long-term relief.[4,5] Tissue engineering has the potential to provide a cure using bio-engineered constructs that can replace damaged or diseased cartilage. It is recognized that the long-term solution to cartilage damage will be an engineered tissue that can substitute for the damaged tissue and take over its load-bearing function.

20.2 Cartilage

Native hyaline cartilage tissue has a three-layered zonal structure comprised of a small amount (~1–5%) of chondrocytes embedded in an extracellular matrix (ECM) (see Figure 1.2 in Chapter 1). The ECM is composed of tissue fluid (~70–80% of wet weight) and structural macromolecules: collagens (~40–60% of dry weight), proteoglycans (~25–35% of dry weight) and non-collagenous proteins and glycoproteins (~15–20% of dry weight).[6] Amongst the collagens, type II is the most abundant (~80%), while types IX and XI occupy ~15% of the total volume. The other collagen types (III, XII, VI, *etc.*) are found in much smaller quantities (~5%).[7,8] Proteoglycans are made of a hyaluronan filament protein core that is attached to multiple glycosaminoglycan (GAG) chains. Each unit of these GAGs has at least one negatively charged carboxylate and sulfate group. These long chains of negatively charged GAG attract cations such as sodium and calcium. Therefore, the typical sodium concentration inside cartilage tissue is higher (~240–300 mM) than that of surrounding tissue fluid (~145 mM). This ion concentration gradient is governed by the Donnan osmotic effect (see Chapter 2).[9,10] Tension created by Donnan osmotic effect is responsible for 50% of cartilage tissue stiffness and is an indicator of cartilage health. Collagen is a charge-neutral macromolecule that forms a cross-linked fibril network inside the tissue. The orientation and composition of these fibers change along the depth of the tissue and provide mechanical stability to the tissue.

The non-calcified cartilage tissue is divided into three zones: superficial zone (SZ; 10–20%), transitional zone (40–60%) and radial or deep zone (RZ; 20–30%) followed by a calcified zone that is partially mineralized cartilage (see Chapter 1). This zone classification is determined according to the collagen fiber orientation. Proteoglycans and collagen are interwoven throughout the tissue depth. Collagen fibers are parallel to the articular

surface in the superficial zone and change their orientation from parallel to perpendicular as we move along the tissue depth. Chondrocytes change their shape, size, and orientation throughout the tissue depth. The amount of proteoglycans increases as we move along the tissue depth, from SZ to RZ. This ordered macromolecular arrangement is important for articular cartilage as a load-bearing tissue.[11] The water plays an important role in the lubricant properties of cartilage, and its content decreases along the tissue depth. Oxygen concentration is also found to decrease through the tissue depth.[12,13]

20.3 Cartilage Tissue Engineering

Cartilage tissue engineering has been an active field of research for the past three decades.[14] In order to create a cartilage-like tissue, tissue engineers employ various strategies that take advantage of the "tissue engineering principle". This includes utilizing a combination of cell sources (*i.e.* chondrocytes or multipotent stem cells), scaffolds (*i.e.* natural, synthetic, or hybrid polymers), growth factors [*i.e.* transforming growth factor (TGF)-β or insulin-like growth factor (IGF)], and cell culture conditions (*i.e.* control of mechanical stimulation, stiffness, porosity, or oxygen tension) to generate a neocartilage tissue with major chondrogenic ECM proteins.[15–17] The major objective of cartilage tissue engineering has been to create a high yield of cartilage ECM right from the beginning after cell seeding. It is well-known that in order to produce a functional cartilage tissue, not only is the amount of generated matrix important, but so is the arrangement of these components within the tissue. This has proved to be more difficult than originally thought, and efforts are underway to achieve the compositional details of engineered cartilage tissue to mimic the native tissue.

20.3.1 Cells

20.3.1.1 Chondrocytes

Chondrocytes, the native cartilage cells, are the most efficient cell types for producing chondrogenic ECM, and therefore are the most desirable cell types for cartilage tissue engineering. Chondrocytes are spherical/ellipsoidal large cell types that produce rich cartilage ECM proteins under the right conditions, *e.g.* mechanical load, hypoxia, *etc.*[18] It has been shown that chondrocytes as scaffold-free pellets produce a large amount of proteoglycans and collagen, type II.[19,20] Chondrocytes do not maintain their spherical phenotypes over the course of tissue regeneration beyond 2–3 weeks. Therefore, chondrocytes embedded in hydrogels such as alginate, gelatin, poly(ethylene glycol)-diacrylate (PEGDA) or other porous hydrogels are attractive choices for maintaining chondrogenic phenotype and improving ECM yield.[16,21–23] It has been shown that chondrocytes seeded in alginate beads maintain their phenotype for up to 8 months.[22]

20.3.1.2 Stem Cells

Despite success in producing chondrogenic ECM with chondrocytes, harvesting enough chondrocytes for expansion and differentiation is challenging because of the limited supply of these cells in natural tissue. Therefore, multipotent mesenchymal stromal/stem cells have been tested and found to be successful in differentiating towards chondrogenic lineage. Research has shown that bone marrow derived and adipose derived stem cells are capable of chondrogenic differentiation when grown as scaffold free pellets or when implanted in various scaffolds.[15,21,24–30] Co-culture of stem cells and chondrocytes has been found to increase the yield of chondrogenic ECM.[21,31]

20.3.2 Scaffolds

Scaffolds provide a template for tissue growth and mechanical stability, and also support cell attachment, differentiation, and proliferation. Therefore, they are widely used in cartilage tissue engineering and regeneration.[32,33] In addition to providing mechanical stability, three-dimensional porous scaffolds provide upkeep of nutrient transport and waste disposal, two important cell functions.[28,34,35] Both natural and synthetic scaffolds have been used in cartilage tissue engineering. Among the natural polymers, collagen, fibrin glue, agarose, alginate, hyaluronic acid, chitosan, and cellulose are some that have been shown to support chondrogenic differentiation of chondrocytes and stem cells.[29,32,36] Ease of tuning mechanical properties, pore volume and surface characteristics encourage increasing use of synthetic and/or composite polymers. A few commonly used polymers are: poly(lactice-*co*-glycolic acid) (PLGA), poly(ethylene glycol) diacrylate (PEGDA), carbon nanotubes and fibers, dacron and teflon, and PuraMatrix™ hydrogels.[33,37] Another common approach is to use biomimetic scaffolds containing chondrogenic ECM that have been shown to promote chondrogenic differentiation of stem cells or chondrocytes without the need of external growth factors.[37–41] Extracellular matrix in cartilage provides a natural scaffold for chondrocytes, allowing decellularized tissues to be used as scaffolds to support and promote chondrogenesis differentiation of cells.[42]

20.3.3 Growth Factors and Growth Strategies

As stated above, one of the goals of cartilage tissue engineering is to produce chondrogenic ECM in an ample amount right after cell seeding at the beginning of tissue growth. This initial success is considered a benchmark for further *in vivo* evaluation of engineered cartilage. Growth factors such as IGF (insulin-like growth factor) and the TGF-β (transforming growth factor beta) family are found to be effective in promoting chondrogenic differentiation of chondrocytes and stem cells, and have thus become a standard in cartilage tissue engineering.[7]

Several growth conditions have been tested and found to be effective for directing chondrogenic differentiation of chondrocytes or stem cells. Cartilage

is an avascular tissue; therefore, it is hypoxic in nature. It has been shown that the hypoxic condition supports a higher yield of chondrogenic ECM of embryonic stem cells.[12,43–45] Sox9 gene transfer and mechanical stimulation also have been shown to stimulate the chondrogenic differentiation of stem cells.[46]

20.3.4 Tissue Growth Assessment

Currently, when tissue-engineered cartilage is being evaluated, the production of proteoglycan and type-II collagen is used as a biomarker for success. These ECM components are assessed using biochemical techniques that include quantitative GAG and collagen assays, gene expression analyses using the quantitative real-time polymerase chain reaction, and histological staining.[16,22,47–49] The mechanical properties of neo-cartilage are typically assessed by confined or unconfined compression or micro/nano indentation.[23,41,50] When scaffolds are implanted in animals, they are removed at different time points and analyzed *ex vivo*.

A typical optimization loop of cartilage tissue engineering and regenerative medicine products is shown in Figure 20.1. The tissue-engineered cartilage is first assessed *in vitro* using the methods described above to gauge the production of primary ECM molecules. Once successful *in vitro*, the process moves to the next step of optimization, first using small animal models then large animal models, each with their own loop of longitudinal immunohistochemical characterization that varies from months to years. Unfortunately, most current characterization methods are destructive and do not have the potential to map the tissue functionality. Therefore, non-invasive assessment techniques are essential for the success of cartilage tissue engineering. Magnetic resonance spectroscopy (MRS) and magnetic resonance imaging (MRI) are leading non-invasive assessment techniques for assessing the tissue growth and production of ECM in cartilage tissue engineering.

Over the past few years, much progress has been made in the non-invasive MRS and MRI characterization of tissue-engineered cartilage.[51–61] The advantage of MRS/MRI techniques is that the techniques developed at preclinical stage can easily be adapted to clinics, as can be seen with current practices of cartilage assessment in clinics.[62,63]

20.4 MRS and MRI in Cartilage Tissue Engineering

The use of MRS and MRI in assessing and monitoring cartilage regeneration is a growing field. The magnetic resonance signal arises from the nuclei that have both angular momentum and magnetic moment (nuclei with odd number of protons and/or neutrons) (see Chapter 3). Table 20.1 lists some commonly nuclear magnetic resonance (NMR)/MRI active nuclei in biological systems in tissue-engineered cartilage. Water-suppressed ^{1}H NMR has been used to visualize the molecular structure of tissue-engineered cartilage. Carbon (^{13}C) NMR also has been used to find the signatures of various

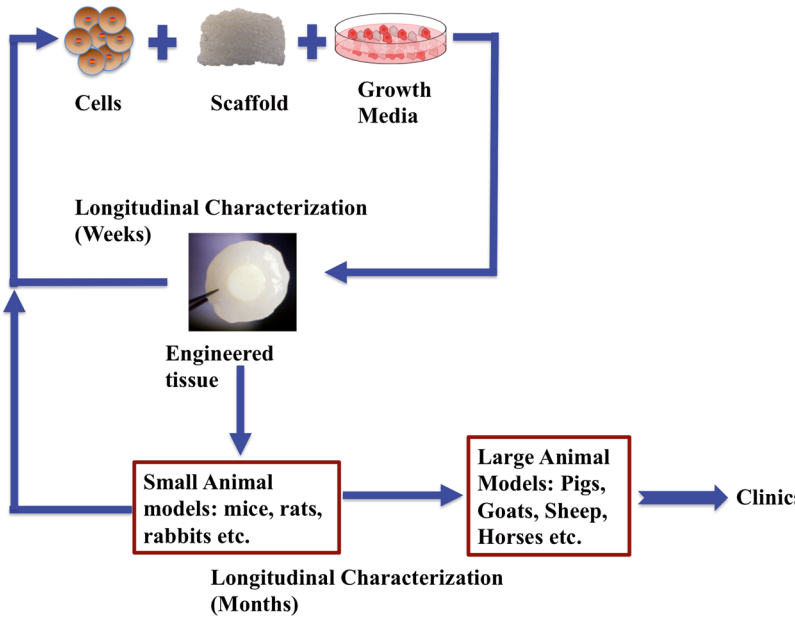

Figure 20.1 Optimization loop for tissue engineering and regenerative medicine products.

Table 20.1 Common magnetic resonance spectroscopy (MRS)/imaging (MRI) active nuclei observed in tissue-engineered cartilage. Both water proton (^{1}H) MRI and sodium (^{23}Na) MRI have been used to assess tissue-engineered cartilage. Water-suppressed ^{1}H nuclear magnetic resonance (NMR), ^{13}C NMR and ^{23}Na multiple-quantum coherence NMR have been used to observe the growth and dynamics in tissue-engineered cartilage.[a]

Nucleus	Atomic number/ atomic mass	Nuclear spin	Gyromagnetic ratio[b] ($\gamma/2\pi$) (MHz T^{-1})	Natural abundance (%)	Relative signal strength (for an equal number of nuclei)	Magnetic resonance contrasts utilized in cartilage tissue engineering
Protons (^{1}H)	1/1	1/2	42.58	99.98	1.000	T_1, T_2, ADC, $T_{1\rho}$, MT
Sodium (^{23}Na)	11/23	3/2	11.26	100.00	0.093	Signal intensity, TQ filter
Carbon (^{13}C)	6/13	1/2	10.71	01.11	0.016	Chemical shift, T_1, T_2

[a]ADC: apparent diffusion coefficient; MT: magnetization transfer; TQ: triple quantum.
[b]T is magnetic field strength in tesla, 1 T = 10 000 Gauss.

proteoglycans and collagen in tissue-engineered cartilage. Sodium (^{23}Na) triple-quantum coherence has been used to assess the tissue anisotropy of different models of tissue-engineered cartilage.

MRI has both the best soft tissue contrast among the available medical imaging modalities and a very high spatial resolution (~20 μm for *in vitro* and ~100 μm for small animal applications). MRI provides three-dimensional maps of engineered tissues that are not available using other assessment techniques. MRI techniques provide real time tissue growth assessment, and will eventually remove or reduce the need for destructive immunohistochemical characterization of engineered cartilage. Water is the most abundant substance in human tissues; therefore, water proton (^{1}H) MRI is the most commonly used MRI modality for cartilage tissue engineering monitoring and assessment. The interaction of water protons with macromolecules provides a window into the biomechanical properties of engineered cartilage tissue. Typical MRI characterization of engineered cartilage relies on changes in T_2-weighted MRI images and changes in magnetic resonance parameters such as water relaxation times; spin-lattice relaxation time (T_1), spin–spin relaxation time (T_2), spin–lattice relaxation time in the rotating frame ($T_{1\rho}$), and the apparent diffusion coefficient (ADC) with tissue growth.[51] Sodium MRI also has been used to assess the GAG amount in stem cell chondrogenesis in a hybrid scaffold system.[58] Carbon and phosphorous MRI also have the potential to shed light on cellular processes and tissue growth dynamics. However, their use in cartilage tissue engineering has not yet been established.

20.5 Magnetic Resonance Accessible Components of Tissue Engineered and Regenerating Cartilage

20.5.1 Assessment of Tissue Growth

20.5.1.1 Water Proton MRI

As stated, the water relaxation times (T_1, T_2, and $T_{1\rho}$), and ADC are commonly used techniques for visualizing and assessing natural cartilage. Figure 20.2 shows high-resolution T_1, T_2, $T_{1\rho}$ and ADC MRI maps of bovine cartilage at 11.7 T and their correlation with the amount of proteoglycans along the depth of the tissue.[64] As shown in the figure, the T_1, $T_{1\rho}$, and ADC are highly correlated with the amount of proteoglycans present in the tissue along the depth, whereas T_2 has a poor correlation with the amount of proteoglycans. It is known that T_2 values in cartilage are influenced by the amount and orientation of collagen in cartilage.[64,65] These relationships, of magnetic resonance parameters with the ECM, prompted a number of MRI studies in cartilage tissue engineering in order to determine a similar relationship between magnetic resonance parameters and the ECM of neocartilage.[55,66,67]

Initial work to correlate magnetic resonance parameters and the ECM of engineered cartilage were established on chondrocyte-based cartilage tissue

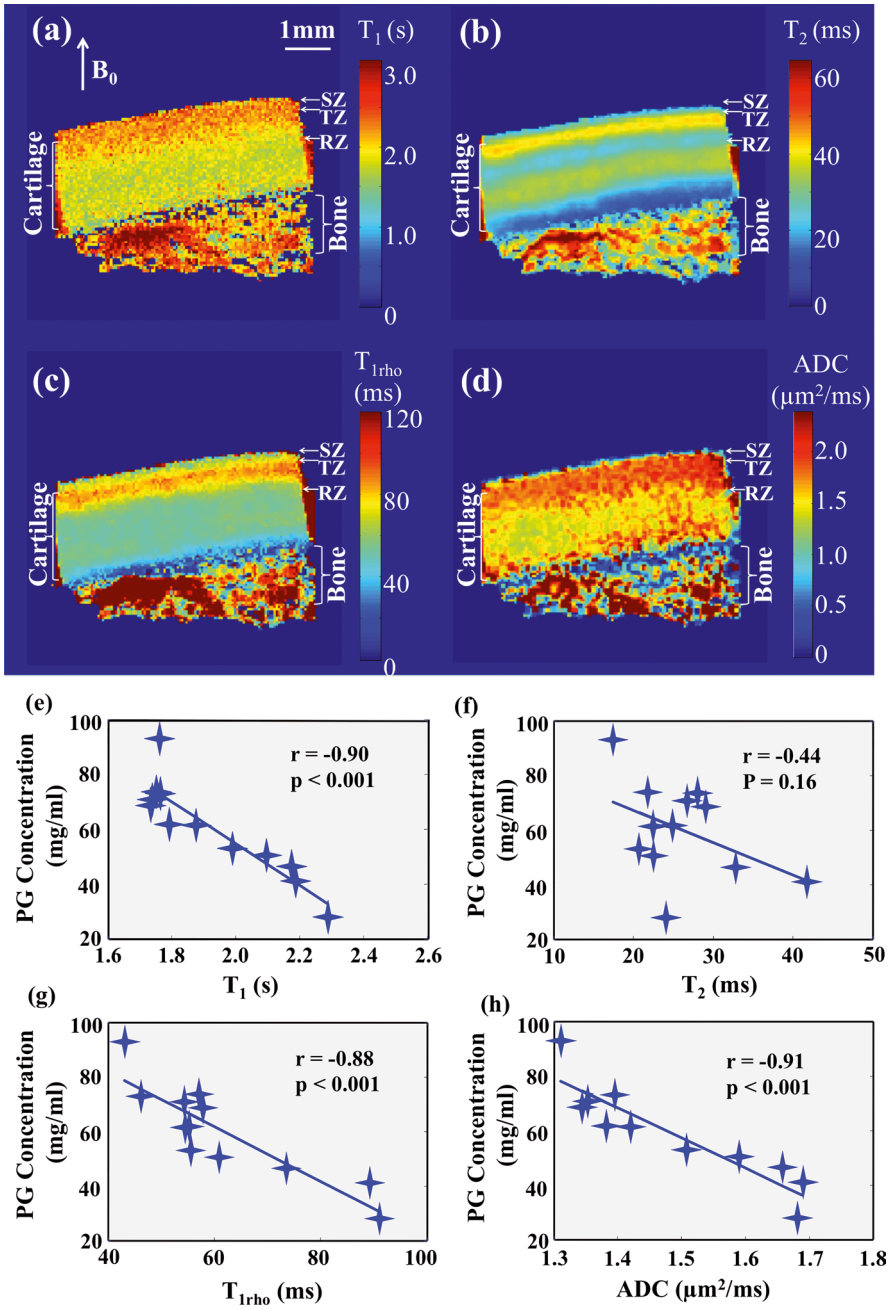

Figure 20.2 (a–d) High-resolution T_1, T_2, $T_{1\rho}$, and apparent diffusion coefficient (ADC) maps of bovine cartilage at 11.7 T. (e–h) Correlation of magnetic resonance parameters with proteoglycan (PG) amount. (Figure adapted from Biomedical Engineering, 42, Z. Yin, Magnetic Resonance Characterization of Tissue Engineered Cartilage *via* Changes in Relaxation Times, Diffusion Coefficient, and Shear Modulus, 137–191, Copyright 2014, with permission from Begell House, Inc.)

engineering, *i.e.* chondrocytes grown as scaffold-free pellets or chondrocytes embedded in a natural or synthetic hydrogel. Both of these cartilage tissue-engineering models produce a large amount of proteoglycans and collagen, type II.[17,18,68] The water relaxation times T_1, T_2, $T_{1\rho}$, and ADC have been shown to decrease with increasing amount of ECM in tissue-engineered cartilage.[55,61,69,70] An example of such correlation is given in Figure 20.3. In this study, chondrocytes were grown as pellets in chondrogenic growth media for three weeks. At each time point (days 3, 7, 14 and 21), three pellets were removed from the media and MRI experiments were performed on them. The samples were placed on top of agar gel to achieve the sample position in the center of the radiofrequency coil. The magnetic resonance parameters are found to be in good correlation with both proteoglycans and collagen.[69,70] However, the magnetic resonance parameters are not specific to any

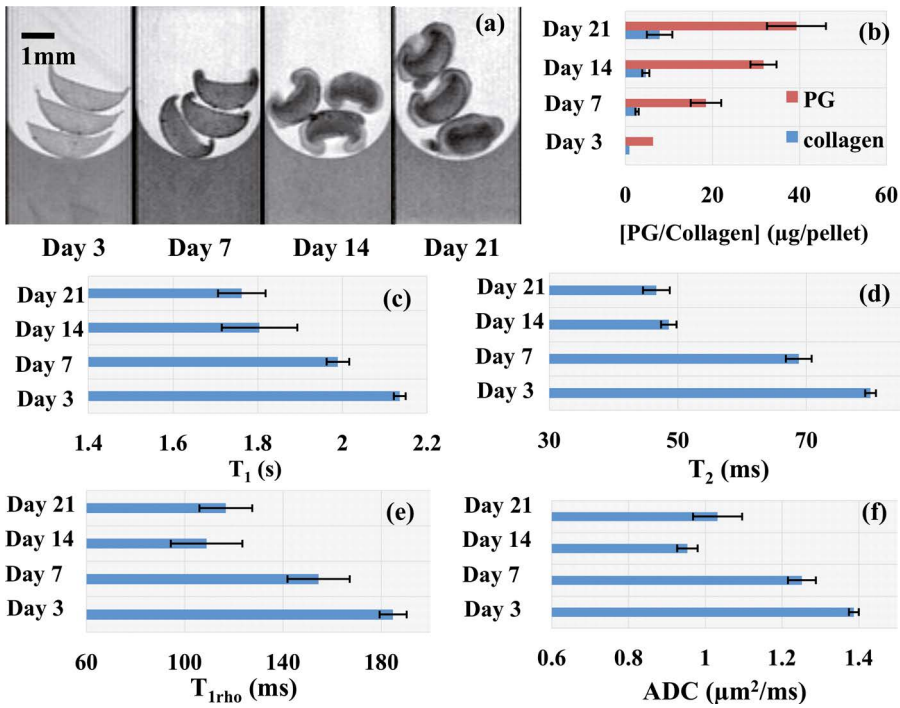

Figure 20.3 Magnetic resonance imaging (MRI) monitoring of chondrocyte pellets over a 3 week incubation period. (a) T_2-weighted MRI images of pellets observed for 3 weeks. The bottom of the tube is filled with agar gel to keep the samples at the center of the radiofrequency coil. The pellet samples are placed on top of this gel and media fills the empty space thus showing a brighter background. The change in (b) proteoglycan (PG) and collagen, (c) T_1, (d) T_2, (e) $T_{1\rho}$, and (f) apparent diffusion coefficient (ADC) over the course of a 3 week culture period clearly indicate the tissue growth. The error bars represent standard deviations. (Figure adapted from Biomedical Engineering, 42, Z. Yin, Magnetic Resonance Characterization of Tissue Engineered Cartilage *via* Changes in Relaxation Times, Diffusion Coefficient, and Shear Modulus, 137–191, Copyright 2014, with permission from Begell House, Inc. and ref. 70.)

single component of cartilage matrix, *i.e.* the amount of proteoglycans or collagen. Similar results have been shown for chondrocytes grown in agarose gel or alginate beads.[55,61] The engineered collagen does not have long and oriented fibers as natural tissues. Thus the relaxation maps (T_1, T_2, and $T_{1\rho}$) only roughly reflect the amount of tissue matrix within the tissue.

In another experiment, we tested the sensitivity of ADC in assessing tissue growth. Bovine chondrocytes were seeded in alginate beads with different cell densities (1, 2 and 4 million cells mL^{-1}) and subjected to chondrogenic differentiation. The ADC of beads along with acellular control was measured for 4 weeks. Figure 20.4 shows the sensitivity of normalized ADC (nADC) in identifying tissue growth as a function of cell seeding density as well as

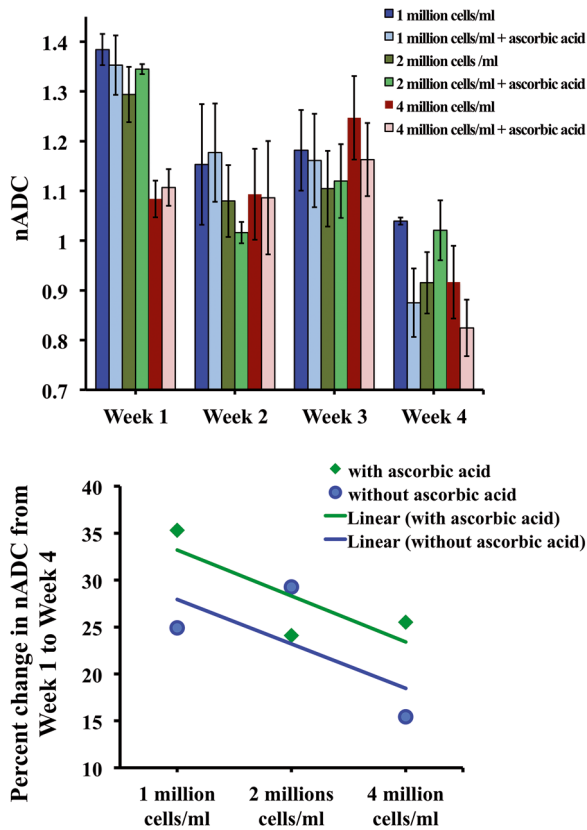

Figure 20.4 Top: change in normalized apparent diffusion coefficient (nADC) as a function of cell seeding density, vitamin co-factor, and culture time. The error bars represent standard error of mean. Bottom: percentage change in nADC as a function of cell seeding density and vitamin co-factor from week 1 to week 4. (© 2014 IEEE. Reprinted, with permission, from M. Kotecha, T. M. Schmid, B. Odintsov and R. Magin, Engineering in Medicine and Biology Society (EMBC), 2014 36th Annual International Conference of the IEEE, Chicago, 26–30 Aug. 2014, 2014.[61])

the vitamin co-factor (ascorbic acid) added to stimulate the growth of collagen, type II for chondrocytes seeded in alginate beads.[61] Here nADC refer to the ADC of chondrogenic alginate beads compared to the acellular alginate beads subjected to the same culture conditions. It is interesting to note that nADC can differentiate the tissue growth between the groups with and without ascorbic acid as well as from low to high cell seeding density. Another interesting fact is that the percentage change in ECM amount from week 1 to week 4 is higher for low cell seeding density.

The correlation between magnetic resonance parameters and increased tissue-engineered matrix is well established in chondrocyte-based cartilage tissue engineering, as shown in Figure 20.3. However, in cases when ECM yield is low and there is also a significant contribution of scaffold in magnetic resonance parameters, this relationship is not obvious. This is a common scenario in stem cells and scaffold-based tissue engineering. In such cases, the magnetic resonance parameters do not seem to change with growing matrix, as observed in our recent works of chondrogenesis of stem cells.[60] Here, the scaffold contribution dominated the magnetic resonance parameters. If we assume that there is no cross-correlation between different contributions arising from ECM, cells, and scaffold, then the relaxation rates are additive and contributions of different components to the relaxation rate can be separated out using the simple algebraic equation as shown below:

$$R_x(\text{ECM + cells}) = R_x(\text{Scaffold + ECM + cells}) - R_x(\text{Scaffold}) \qquad (20.1)$$

where $R_x = 1/T_x$, $x = 1$ or 2.

Figure 20.5 shows the stem cell chondrogenic matrix assessment for 4 weeks of growth using MRI. As shown in the figure, once the scaffold contribution is removed, both mean T_1 and T_2 are correlated with the mean amount of the GAG to DNA ratio (GAG/DNA); here the Pearson correlation coefficient was calculated as 0.98 and 0.62, respectively. We have shown recently that this biomaterial filtering method can also be used to observe chondrogenesis *in vivo*.[38]

20.5.2 Assessment of Tissue Anisotropy and Dynamics

Engineered cartilage tissue morphology is often different from the native cartilage tissue because of different growth pathways. The natural tissue has long and oriented collagen fibers in large quantities, and proteoglycans, trapped in the collagen network, in a smaller quantity. In contrast, engineered tissues may have a higher cell density, an elevated proteoglycan amount, and short collagen fibers with random orientation owing to a small growth time of few weeks to few months.[52] This may also be due to lack of directed mechanical loading; however, we are not aware of any research that shows that mechanical loading produces long and oriented collagen fibers compared to non-mechanical settings of tissue culture. In addition, engineered tissue also possesses a biocompatible scaffold specifically chosen

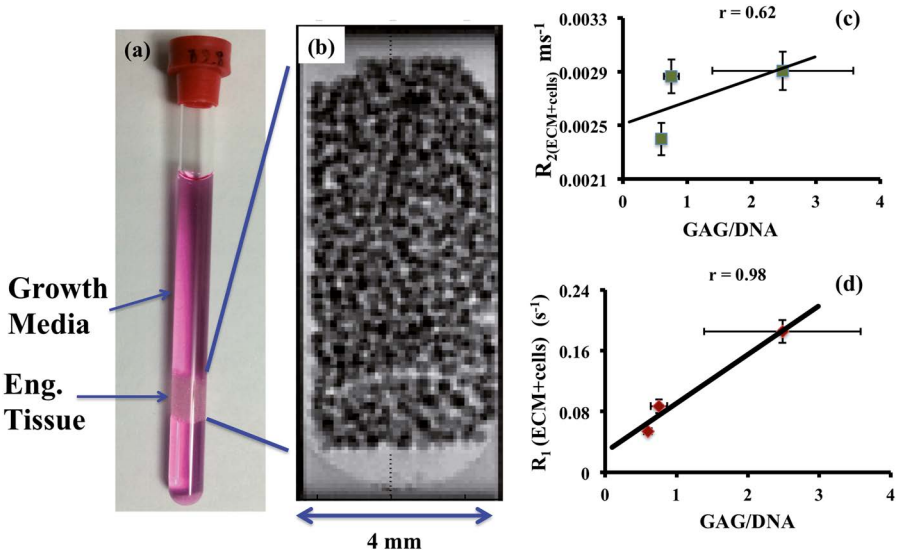

Figure 20.5 (a) Tissue-engineered chondrogenic matrix made out of PLGA-Puramatrix™ hydrogel in a 5 mm magnetic resonance imaging tube. (b) T_2 weighted image of tissue-engineered chondrogenic matrix. The matrix has one side more porous and other side less porous for subsequent use in osteochondral tissue engineering. (c) Correlation between average glycosaminoglycan (GAG)/DNA and the corresponding average calculated relaxation rates R_2 (=1/T_2). (d) Correlation between average GAG/DNA and average calculated relaxation rates R_1 (=1/T_1). (Figure adapted from ref. 60.)

to provide the right growth environment for cells and for mechanical support. This results in variable tissue morphology, as shown in Figure 20.6. The correct assessment of tissue anisotropy and the macromolecular environment is therefore an important predictor of the tissue's functional properties.

20.5.2.1 Proton NMR Spectroscopy

NMR spectroscopic studies have contributed significantly to our understanding of the complex macromolecular structure and dynamics of cartilage tissue.[71–75] The mobility of macromolecules, *i.e.* collagen fibers and proteoglycans, plays an important role in the load-bearing functional properties of cartilage. Using ^{13}C magic angle spinning NMR relaxation, Huster *et al.* studied the mobility of chondroitin sulfate and collagen in bovine nasal cartilage and concluded that proteoglycans in cartilage are relatively flexible in a rigid collagen network.[76] This is also evident from the ^{1}H NMR of bovine cartilage tissue showing a sharp *N*-acetyl peak coming from proteoglycans at 2 ppm.[75] Using ^{13}C NMR, Schulz *et al.* demonstrated the presence of chondroitin sulfate in the cartilage tissue-engineered constructs.[49]

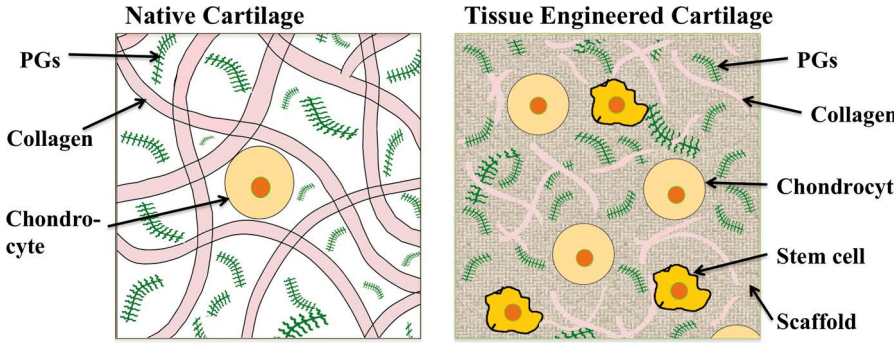

Figure 20.6 Schematic diagram showing gross morphological differences between natural and tissue-engineered cartilage. The natural cartilage has a small number of chondrocytes (~1%), long and oriented collagen type II fibers (~20%), and a small number of proteoglycans (PGs; ~5%). In contrast, tissue-engineered cartilage may have a higher number of cells, both chondrocytes and stem cells, short and random oriented collagen fibers, and may have an elevated amount of proteoglycans. In addition, tissue-engineered cartilage also has a scaffold that is chosen for its biomechanical properties. (Figure adapted from ref. 60.)

Figure 20.7a shows the water-suppressed ^{1}H NMR spectra demonstrating chondrogenesis of human marrow stromal cells (HMSCs) seeded into 1:1 chitosan:collagen type I scaffolds after 4 weeks of culture time. The chondrogenesis of HMSCs was confirmed using immunohistochemical staining. Figure 20.7b shows the water-suppressed ^{1}H NMR spectra of chondrocyte pellets for the 4 week culture period.[77] These pellets had a high yield of proteoglycans and collagen, as presented in Figure 20.3b. Note that when compared to natural tissue, the *N*-acetyl resonance at 2 ppm in these engineered tissues is broad or non-existent (Figure 20.7).[75] This is surprising, given the higher production of proteoglycans compared to collagen in chondrocyte pellets, as shown in Figure 20.3b. We suspect that this broad resonance might be due to non-mobile GAG chains. Our NMR studies of engineered cartilage (Figure 20.7) show that engineered tissues have a different morphology from that of native tissue. Further investigations of the mobility of these macromolecules in a controlled study will provide us with an insight into the tissue architecture of neocartilage at the early stage. This early-stage morphology of engineered tissue is expected to guide ultimate functional properties of engineered cartilage.

20.5.2.2 Sodium TQ NMR

Quadrupolar spin probes such as sodium with spin 3/2 possess an electric quadrupole moment (Q). The Q interacts with local electric field gradients (EFG) at the site of the nucleus, making it extremely sensitive to the local environment. In isotropic solution, the average interaction between Q and EFG is

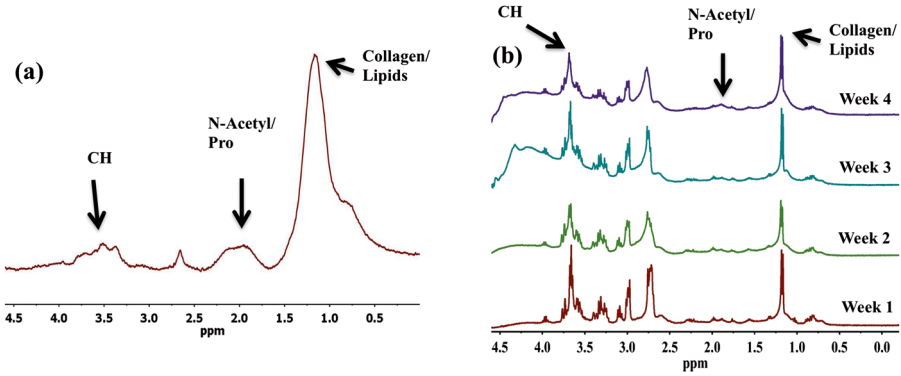

Figure 20.7 (a) Water-suppressed ^{1}H nuclear magnetic resonance (NMR) spectra of tissue-engineered cartilage at 9.4 T at the end of the 4 week culture period. The production of proteoglycans and collagen were independently confirmed using safranin O staining and Fourier transform infrared imaging. (b) Water-suppressed ^{1}H NMR spectra of 4 weeks of growth of chondrocyte pellets. The production of proteoglycans and collagen was confirmed using biochemical assays as shown in Figure 20.3(b). Note the missing *N*-acetyl peak at 2 ppm, even though the amount of proteoglycan was higher than collagen.

zero; however, in an anisotropic or ordered environment the EFG at the nucleus is non-zero. In such cases, a residual quadrupolar coupling can be observed through the multiple-quantum coherence NMR signal (see also Chapter 9). Here, the relaxation time is biexponential with one short (T_f) and one long (T_s) component owing to the satellite ($\pm 3/2 \leftrightarrow \pm 1/2$) and central transitions ($-1/2 \leftrightarrow +1/2$). The triple-quantum coherence signal can be written as:[52]

$$S(\tau,t) \approx M_0 \frac{9}{80}\left[\left\{e^{-(R_f - i\omega_Q)\tau} - 2e^{-R_s\tau} + e^{-(R_f + i\omega_Q)\tau}\right\}\left\{e^{-(R_f - i\omega_Q)t} - 2e^{-R_s t} + e^{-(R_f + i\omega_Q)t}\right\}\right] \tag{20.2}$$

where R_f ($=1/T_f$) and R_s ($=1/T_s$) are the fast and slow decaying components of transverse relaxation rate and ω_Q is the residual average quadrupolar coupling. The average quadrupolar coupling, ω_Q, is zero in an isotropic environment and ≈2–3 kHz in natural cartilage.[52,78] Figure 20.8 shows an example of triple-quantum coherence signal for three different engineered cartilage tissues and their best fit using eqn (20.2). Using the calculated fast and the slow relaxation times, the motional averaging parameter $\omega_0\tau_c$ can be calculated thus:[79]

$$\omega_0\tau_c = \left[\frac{1}{8}\left\{5\frac{R_f}{R_s} - 9 + \left(\left(5\frac{R_f}{R_s}\right)^2 - 58\frac{R_f}{R_s} + 49\right)^{1/2}\right\}\right]^{1/2} \tag{20.3}$$

where ω_0 is the Larmor frequency for sodium ions and τ_c is rotational correlation time that represents how fast or slow sodium ions can tumble depending

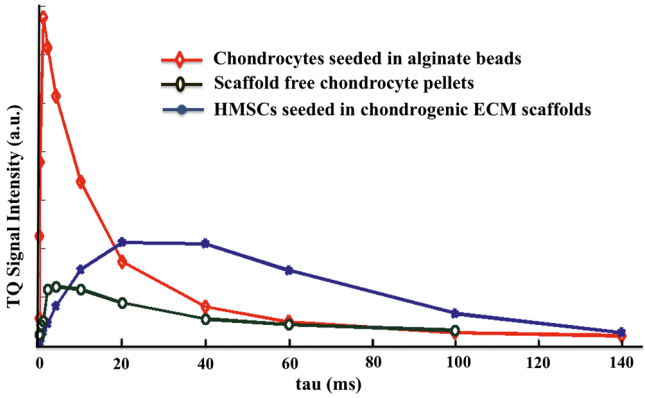

Figure 20.8 The sodium triple quantum coherence build-up curve for three cartilage tissue-engineering constructs at 9.4 T (^{1}H frequency = 400 MHz). Even though sodium ions bind with proteoglycans and relaxation times can be correlated with the amount of proteoglycans in natural tissue, its relaxation is strongly influenced by the environment in engineered cartilage that includes scaffold, cells, proteoglycans, and collagen. HMSC: human marrow stromal cells; ECM: extracellular matrix. (Figure adapted from ref. 52.)

upon its environment. The correlation time, τ_c, is a measure of ECM composition in the cartilage tissue, since the internal structure of the tissue defines the molecular motion in the tissue. Together, the motional averaging parameter, $\omega_0\tau_c$, and average quadrupolar coupling, ω_Q, provide information about dynamics and tissue anisotropy.

We applied sodium triple-quantum (TQ) coherence NMR spectroscopy to study the dynamics and anisotropy in tissue-engineered cartilage.[52] Three different types of tissue-engineered constructs were studied: chondrocyte pellets, chondrocytes seeded in alginate beads, and human marrow stromal cells seeded in ECM-integrated biomimetic scaffolds. As shown in Table 20.2 and Figure 20.8, the main findings of this study were: (1) smaller values of τ_c and ω_Q, indicating faster sodium motion and reduced tissue anisotropy in engineered cartilage compared to native cartilage tissue, and (2) the TQ coherence build-up curves in engineered cartilage were strongly influenced by the environment. The reduced anisotropy is a direct result of random orientation and short collagen fibers in engineered cartilage in contrast to the well organized long collagen fibers in natural cartilage. The fast sodium ion motion could mean that there is significantly less binding between proteoglycans and sodium ions in engineered cartilage. This may be the result of the dense packing of proteoglycans and collagen in engineered cartilage. The electrostatic interaction between positively charged ions such as sodium, and negatively charged proteoglycans is responsible for 50% of the tissue's equilibrium compressive stiffness and is an important component in the special viscoelastic properties of cartilage.[9] The long and oriented collagen fibers

Table 20.2 The average quadrupolar coupling ω_Q and motional parameter ($\omega_0\tau_c$) for scaffold-free and scaffold-based tissue-engineered cartilage and native cartilage at 400 MHz (9.4 T) after 4 weeks of culture time. Both the correlation time τ_c, and the average quadrupolar coupling ω_Q are smaller in engineered tissues than native tissue. Values are given with standard parameter error of fitting. The * value is not included in the table because the error in fitting exceeded the calculated parameter value many fold. The absence of triple-quantum build-up signifies the isotropic environment for sodium ions. HMSCs: human marrow stromal cells; ECM: extracellular matrix (Table adapted from ref. 52.).

	Human HMSCs in ECM embedded scaffolds		Bovine chondrocytes in alginate beads		Bovine chondrocytes in pellets		Human cartilage explants	
	ω_Q (Hz)	$\omega_0\tau_c$	ω_Q (Hz)	$\omega_0\tau_c$	ω_Q (Hz)	$\omega_0\tau_c$	ω_Q (Hz)	$\omega_0\tau_c$
After 4 weeks of culture	*	4.65 ± 0.29	628 ± 458	6.5 ± 0.14	No TQ build-up	No TQ build-up	2463 ± 798	8.42 ± 0.24

provide the necessary structural and mechanical support for the load-bearing viscoelastic functional properties of cartilage. Therefore, we call τ_c and ω_Q "functional assessment parameters". The extent of deviation of these functional assessment parameters from native cartilage parameters can be termed as the lack of functionality (or lack of load-bearing capabilities) of tissue-engineered cartilage. These results show that the choice of scaffold dictates the composition of emerging ECM in engineered tissues and, ultimately, also influences the functional assessment parameters.

The question we ask is this: can this information be integrated into the outcome prediction in cartilage tissue engineering? Such information is not currently a part of the routine assessment of engineered cartilage tissues, but could become an important tool for crafting functional engineered cartilage.

20.5.2.3 Diffusion Tensor Imaging

Mean diffusivity (MD) and fractional anisotropy (FA) derived from diffusion tensor imaging (DTI) can provide information about nutrient transport and tissue anisotropy in tissue-engineered cartilage. In an experiment, where DTI experiments were performed on both chondrogenic constructs ($n = 3$) and corresponding acellular constructs ($n = 3$) after 4 weeks of tissue growth, we found that while the MD reduced slightly in chondrogenic constructs as a sign of tissue growth, the FA remained low and almost unchanged during the growth period. These results, presented in Table 20.3 are in agreement with our sodium TQ results, showing lower anisotropy in tissue-engineered cartilage. The advantage of the DTI experiment in assessing tissue anisotropy is the high available water content in engineered tissues, and thus a

Table 20.3 Mean diffusivity (MD) and fractional anisotropy (FA) of chondrogenic constructs and acellular control scaffolds. The chondrogenic constructs were prepared by seeding human marrow derived stromal cells in PLGA-Puramatrix™ hydrogel similar to that shown in Figure 20.6. One side of the constructs was more porous while the other side was less porous for their subsequent use in osteochondral tissue engineering. Average number of voxels in these groups was 1270 ± 156.

	Chondrogenic ($n = 3$)		Acellular control ($n = 3$)	
	Porous	Non-porous	Porous	Non-porous
MD ± SD ($*10^{-3}$ mm^2 s^{-1})	1.59 ± 0.06	1.49 ± 0.11	1.69 ± 0.06	1.60 ± 0.12
FA ± SD	0.20 ± 0.07	0.23 ± 0.07	0.19 ± 0.07	0.22 ± 0.01

high signal-to-noise ratio in images. However, DTI images suffer from partial volume effects in MRI acquisition as well as lack of calibration for assigning the correct FA to the tissue component of engineered tissues.

20.5.3 Assessment of GAG Amount

20.5.3.1 Sodium MRI

In previous sections, we explained that water relaxation times and ADC parameters provide the first assessment of tissue growth in engineered cartilage. This is an important first step in tissue assessment; however, water magnetic resonance parameters in tissue-engineered cartilage are nonspecific and can be influenced by a number of factors within the tissue continuum, such as the interaction of water with cell density, choice of scaffold, amount of both proteoglycans and collagen, ratio of free to bound water, and cross relaxation. Therefore, development of ECM-specific magnetic resonance techniques for quantitative assessment is of high importance. Sodium ions bind to negatively charged proteoglycans in cartilage tissue, therefore sodium MRI has been used extensively to assess cartilage integrity and to quantify proteoglycan loss in the case of osteoarthritis.[10,80–82] However, its use for the evaluation of tissue-engineered cartilage is still in its infancy. For the first time, our group has demonstrated that sodium MRI can be used for assessing the amount of GAG in a tissue-engineered cartilage.[58] The difference between natural and engineered cartilage tissue assessment using sodium MRI is noteworthy and should be taken into account when generalizing this method. Healthy natural cartilage has a high GAG level (~40–70 mg mL^{-1}), whereas typical GAG production in the early stages of growth in engineered cartilage is smaller by at least two orders of magnitude.[10,81] Therefore, the fixed charge density (FCD) for engineered cartilage may be smaller by two orders of magnitude in early stages when compared to natural tissue. In addition, depending upon the choice of growth strategy, scaffold and cells with low sodium concentration can reduce the final signal strength. Figure 20.9 shows an example of sodium MRI assessment using these strategies.

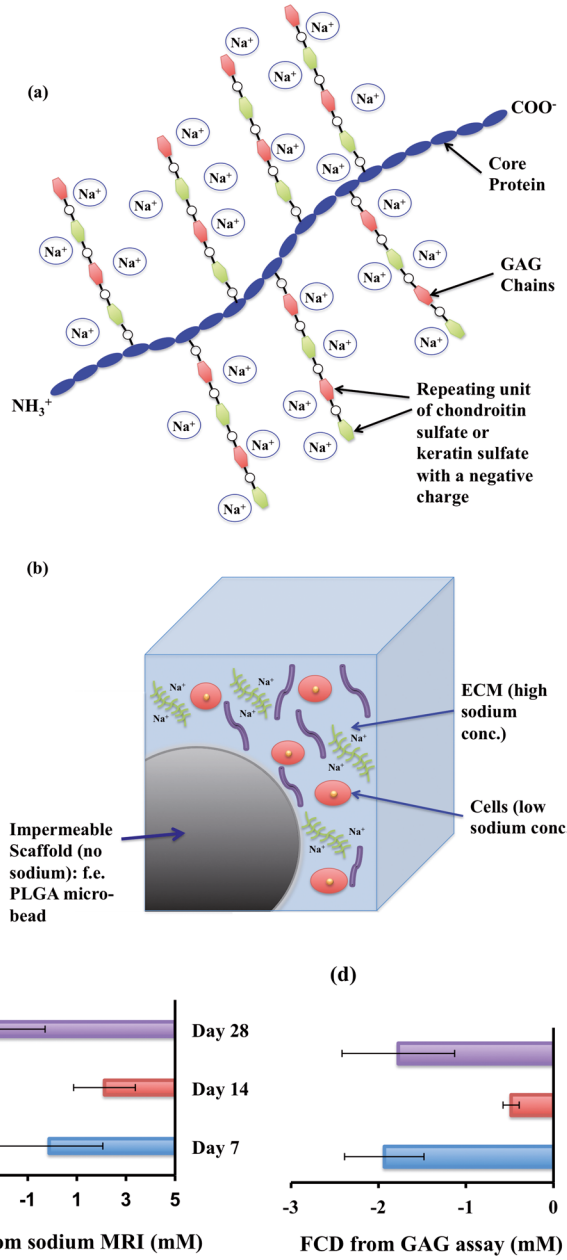

Figure 20.9 (a) Schematic diagram of a proteoglycan with negatively charged glycosaminoglycan (GAG) chains. These negatively charged GAG chains attract sodium ions, therefore, the concentration of sodium is higher in cartilage. (b) Schematic diagram of sodium magnetic resonance imaging (MRI) voxel in a tissue-engineered cartilage matrix. As shown in the figure, the scaffold could occupy a significant voxel volume. Calculated fixed charge density (FCD) at day 7, day 14 and day 28 from (c) the sodium MRI and (d) the GAG assay. The bar represents standard error in both cases. The Pearson correlation coefficient between these two methods was found to be 0.79. ((a) inspired by https://wikispaces.psu.edu/display/230/ and (b–d) reproduced with permission from ref. 58. © 2016 Biomedical Engineering Society. With kind permission from Springer Science and Business Media.)

As shown in the figure, the FCD derived from the sodium MRI is highly correlated with the FCD derived from the GAG assay after taking into account the volumes occupied by scaffolds and cells within the MRI voxel.[58]

20.6 Future Directions

Magnetic resonance in cartilage tissue engineering has come a long way and has shown promise to provide a universal assessment of engineered cartilage tissue growth. This includes an assessment of tissue matrix, tissue anisotropy, and GAG all non-invasively and in real time. The future of the magnetic resonance assessment of tissue-engineered cartilage looks promising and a few clear directions can be thought out.

20.6.1 New Biomaterials

New biomaterials offer the advantages of close tuning of mechanical properties of engineered tissues. Magnetic resonance techniques need to keep up with the pace with which new materials are invented and introduced for cartilage tissue engineering research. A national database of magnetic resonance properties (spectra, relaxation times, and water diffusion coefficients) will expedite the application of magnetic resonance in cartilage tissue engineering in clinics.

20.6.2 Magnetic Resonance Standards

Current methods of predicting tissue growth using MRI rely on the use of water magnetic resonance relaxation times (T_1 and T_2) and ADC; however, the range of change in these parameters is ambiguous and depends on the choice of tissue growth strategies as well as experiment protocols. It is found that for chondrocyte-based and scaffold-free cartilage tissue engineering, these parameters fall monotonically with the production of proteoglycans and collagen; however, the change is diminutive in the case of stem-cell and scaffold-based cartilage tissue engineering. Therefore, there is a strong need to develop standards to define and assign cartilage tissue growth using MRI. This initiative and an American Society for Testing and Materials standard (ASTM) document for the preclinical assessment of engineered cartilage tissue using MRI is under development.

20.6.3 ECM-Specific Techniques

The first measure of success for cartilage tissue engineering is the high yield of two major ECM macromolecules; proteoglycans and collagen, type II. Non-invasive assessment of these ECM components is the major goal of MRI. In Section 20.5.3, we showed that sodium MRI-derived FCD is in close agreement with FCD derived from GAG assays. Sodium MRI offers an unambiguous assessment; however, its low signal-to-noise ratio is a challenge. A water

MRI-based technique such as GAG-based chemical exchange saturation transfer (GAG-CEST) offers a strong alternative and should be investigated further.[83]

20.7 Summary

In this chapter, we have shown that several magnetic resonance techniques offer evaluation of stem cell and chondrocyte differentiation towards chondrogenic lineage with and without the presence of scaffolds. Using these techniques, we can assess the tissue growth, tissue anisotropy and the GAG produced. These techniques offer hope that we will not need destructive assessment techniques in the future and a promise that MRS and MRI have the capabilities of providing functional assessment both *in vitro* and *in vivo*. Further work is needed in standardizing these techniques across various tissue growth strategies, magnetic field strength, choice of experimental protocols, and various animal models that are currently used for the investigation of cartilage tissue engineering and regeneration.

References

1. J. Qin, K. A. Theis, K. E. Barbour, C. G. Helmick, N. A. Baker and T. J. Brady, *Impact of Arthritis and Multiple Chronic Conditions on Selected Life Domains — United States, 2013*, Center for Disease Control and Prevention, 2015.
2. B. L. Clair, A. R. Johnson and T. Howard, *Foot Ankle Spec.*, 2009, **2**, 179–188.
3. T. A. Ahmed and M. T. Hincke, *Tissue Eng., Part B*, 2010, **16**, 305–329.
4. K. Mithoefer, K. Hambly, S. Della Villa, H. Silvers and B. R. Mandelbaum, *Am. J. Sports Med.*, 2009, **37**(suppl. 1), 167S–176S.
5. J. Duchow, T. Hess and D. Kohn, *Am. J. Sports Med.*, 2000, **28**, 24–27.
6. J. A. Buckwalter and H. J. Mankin, *Instr. Course Lect.*, 1998, **47**, 477–486.
7. M. Demoor, D. Ollitrault, T. Gomez-Leduc, M. Bouyoucef, M. Hervieu, H. Fabre, J. Lafont, J. M. Denoix, F. Audigie, F. Mallein-Gerin, F. Legendre and P. Galera, *Biochim. Biophys. Acta*, 2014, **1840**, 2414–2440.
8. D. Eyre, *Arthritis Res.*, 2002, **4**, 30–35.
9. L. M. Lesperance, M. L. Gray and D. Burstein, *J. Orthop. Res.*, 1992, **10**, 1–13.
10. E. M. Shapiro, A. Borthakur, A. Gougoutas and R. Reddy, *Magn. Reson. Med.*, 2002, **47**, 284–291.
11. J. A. Buckwalter, H. J. Mankin and A. J. Grodzinsky, *Instr. Course Lect.*, 2005, **54**, 465–480.
12. S. Saini and T. M. Wick, *Tissue Eng.*, 2004, **10**, 825–832.
13. B. Fermor, S. E. Christensen, I. Youn, J. M. Cernanec, C. M. Davies and J. B. Weinberg, *Eur. Cells Mater.*, 2007, **13**, 56–65; discussion 65.
14. R. A. Somoza, J. F. Welter, D. Correa and A. I. Caplan, *Tissue Eng., Part B*, 2014, **20**, 596–608.
15. R. S. Tuan, G. Boland and R. Tuli, *Arthritis Res. Ther.*, 2003, **5**, 32–45.
16. B. Petit, K. Masuda, A. L. DSouza, L. Otten, D. Pietryla, D. J. Hartmann, N. P. Morris, D. Uebelhart, T. M. Schmid and E. J. M. A. Thonar, *Exp. Cell Res.*, 1996, **225**, 151–161.

17. K. Schrobback, T. J. Klein, M. Schuetz, Z. Upton, D. I. Leavesley and J. Malda, *J. Orthop. Res.*, 2011, **29**, 539–546.
18. S. Thirion and F. Berenbaum, *Methods Mol. Med.*, 2004, **100**, 1–14.
19. Y. C. Cheuk, M. W. Wong, K. M. Lee and S. C. Fu, *J. Orthop. Res.*, 2011, **29**, 1343–1350.
20. Z. Zhang, J. M. McCaffery, R. G. Spencer and C. A. Francomano, *J. Anat.*, 2004, **205**, 229–237.
21. N. Georgi, C. van Blitterswijk and M. Karperien, *Tissue Eng., Part A*, 2014, **20**, 2513–2523.
22. S. Chubinskaya, K. Huch, M. Schulze, L. Otten, M. B. Aydelotte and A. A. Cole, *J. Histochem. Cytochem.*, 2001, **49**, 1211–1220.
23. S. J. Bryant, K. A. Davis-Arehart, N. Luo, R. K. Shoemaker, J. A. Arthur and K. S. Anseth, *Macromolecules*, 2004, **37**, 6726–6733.
24. P. H. Chao, W. Grayson and G. Vunjak-Novakovic, *J. Orthop. Sci.*, 2007, **12**, 398–404.
25. S. Hofmann, S. Knecht, R. Langer, D. L. Kaplan, G. Vunjak-Novakovic, H. P. Merkle and L. Meinel, *Tissue Eng.*, 2006, **12**, 2729–2738.
26. K. Johnson, S. Zhu, M. S. Tremblay, J. N. Payette, J. Wang, L. C. Bouchez, S. Meeusen, A. Althage, C. Y. Cho, X. Wu and P. G. Schultz, *Science*, 2012, **336**, 717–721.
27. W. J. Li, R. Tuli, X. Huang, P. Laquerriere and R. S. Tuan, *Biomaterials*, 2005, **26**, 5158–5166.
28. Y. Wang, U. J. Kim, D. J. Blasioli, H. J. Kim and D. L. Kaplan, *Biomaterials*, 2005, **26**, 7082–7094.
29. K. Yoneno, S. Ohno, K. Tanimoto, K. Honda, N. Tanaka, T. Doi, T. Kawata, E. Tanaka, S. Kapila and K. Tanne, *J. Biomed. Mater. Res., Part A*, 2005, **75**, 733–741.
30. L. Meinel, S. Hofmann, V. Karageorgiou, L. Zichner, R. Langer, D. Kaplan and G. Vunjak-Novakovic, *Biotechnol. Bioeng.*, 2004, **88**, 379–391.
31. R. L. Dahlin, L. A. Kinard, J. Lam, C. J. Needham, S. Lu, F. K. Kasper and A. G. Mikos, *Biomaterials*, 2014, **35**, 7460–7469.
32. L. Cen, W. Liu, L. Cui, W. Zhang and Y. Cao, *Pediatr. Res.*, 2008, **63**, 492–496.
33. F. T. Moutos and F. Guilak, *Biorheology*, 2008, **45**, 501–512.
34. W. J. Li, R. Tuli, C. Okafor, A. Derfoul, K. G. Danielson, D. J. Hall and R. S. Tuan, *Biomaterials*, 2005, **26**, 599–609.
35. J. K. Wise, A. L. Yarin, C. M. Megaridis and M. Cho, *Tissue engineering. Part A*, 2009, **15**, 913–921.
36. Y. Kirilak, N. J. Pavlos, C. R. Willers, R. Z. Han, H. T. Feng, J. K. Xu, N. Asokananthan, G. A. Stewart, P. Henry, D. Wood and M. H. Zheng, *Int. J. Mol. Med.*, 2006, **17**, 551–558.
37. S. Q. Liu, Q. Tian, J. L. Hedrick, J. H. Po Hui, P. L. Ee and Y. Y. Yang, *Biomaterials*, 2010, **31**, 7298–7307.
38. S. Ravindran, M. Kotecha, C.-C. Huang, A. Ye, P. Pothirajan, Z. Yin, R. Magin and A. George, *Biomaterials*, 2015, **71**, 58–70.
39. K. E. M. Benders, P. R. v. Weeren, S. F. Badylak, D. B. F. Saris, W. J. A. Dhert and J. Malda, *Trends Biotechnol.*, 2013, **31**, 169–176.

40. T. J. Klein, J. Malda, R. L. Sah and D. W. Hutmacher, *Tissue Eng., Part B*, 2009, **15**, 143–157.
41. F. T. Moutos, L. E. Freed and F. Guilak, *Nat. Mater.*, 2007, **6**, 162–167.
42. C. W. Cheng, L. D. Solorio and E. Alsberg, *Biotechnol. Adv.*, 2014, **32**, 462–484.
43. E. J. Koay and K. A. Athanasiou, *Osteoarthritis Cartilage*, 2008, **16**, 1450–1456.
44. K. Schrobback, J. Malda, R. W. Crawford, Z. Upton, D. I. Leavesley and T. J. Klein, *Tissue Eng., Part A*, 2012, **18**, 920–933.
45. K. Schrobback, T. J. Klein, R. Crawford, Z. Upton, J. Malda and D. I. Leavesley, *Cell Tissue Res.*, 2012, **347**, 649–663.
46. L. Kupcsik, M. J. Stoddart, Z. Li, L. M. Benneker and M. Alini, *Tissue Eng., Part A*, 2010, **16**, 1845–1855.
47. S. Chandrasekhar, M. A. Esterman and H. A. Hoffman, *Anal. Biochem.*, 1987, **161**, 103–108.
48. C. D. Hoemann, *Methods Mol. Med.*, 2004, **101**, 127–156.
49. R. Schulz, S. Hohle, G. Zernia, M. Zscharnack, J. Schiller, A. Bader, K. Arnold and D. Huster, *J. Nanosci. Nanotechnol.*, 2006, **6**, 2368–2381.
50. C. J. Little, N. K. Bawolin and X. Chen, *Tissue Eng., Part B*, 2011, **17**, 213–227.
51. M. Kotecha, D. Klatt and R. L. Magin, *Tissue Eng., Part B*, 2013, **19**, 470–484.
52. M. Kotecha, S. Ravindran, T. M. Schmid, A. Vaidyanathan, A. George and R. L. Magin, *NMR Biomed.*, 2013, **26**, 709–717.
53. H. H. Xu, S. F. Othman and R. L. Magin, *J. Biosci. Bioeng.*, 2008, **106**, 515–527.
54. S. Miyata, K. Homma, T. Numano, T. Tateishi and T. Ushida, *J. Biomech. Eng.*, 2010, **132**, 071014.
55. S. Miyata, T. Numano, K. Homma, T. Tateishi and T. Ushida, *J. Biomech.*, 2007, **40**, 2990–2998.
56. S. Ramaswamy, J. B. Greco, M. C. Uluer, Z. J. Zhang, Z. L. Zhang, K. W. Fishbein and R. G. Spencer, *Tissue Eng., Part A*, 2009, **15**, 3899–3910.
57. S. Ramaswamy, M. C. Uluer, S. Leen, P. Bajaj, K. W. Fishbein and R. G. Spencer, *Tissue Eng., Part C*, 2008, **14**, 243–249.
58. S. Majumdar, P. Pothirajan, D. L. Dorcemus, S. Nukavarapu and M. Kotecha, *Ann. Biomed. Eng.*, 2016, **44**, 1120–1127.
59. P. Pothirajan, S. Ravindran, A. George, R. Magin and M. Kotecha, *presented in part at the Engineering in Medicine and Biology Society (EMBC), 2014 36th Annual International Conference of the IEEE*, Chicago, pp. 26–30, 2014.
60. P. Pothirajan, D. L. Dorcemus, S. Nukavarapu and M. Kotecha, *presented in part at the Engineering in Medicine and Biology Society (EMBC), 2014 36th Annual International Conference of the IEEE*, Chicago, 2014.
61. M. Kotecha, T. M. Schmid, B. Odintsov and R. Magin, *presented in part at the Engineering in Medicine and Biology Society (EMBC), 2014 36th Annual International Conference of the IEEE*, Chicago, pp. 26–30, 2014.

62. B. Sharma, S. Fermanian, M. Gibson, S. Unterman, D. A. Herzka, B. Cascio, J. Coburn, A. Y. Hui, N. Marcus, G. E. Gold and J. H. Elisseeff, *Sci. Transl. Med.*, 2013, **5**, 167ra6.
63. M. D. Crema, F. W. Roemer, M. D. Marra, D. Burstein, G. E. Gold, F. Eckstein, T. Baum, T. J. Mosher, J. A. Carrino and A. Guermazi, *Radiographics*, 2011, **31**, 37–61.
64. Z. Yin, M. Kotecha, T. M. Schmid and R. L. Magin, *presented in part at the The 11th International Conference on Magnetic Resonance Microscopy (ICMRM)*, Beijing, China, 2011.
65. S. F. Othman, J. Li, O. Abdullah, J. J. Moinnes, R. L. Magin and C. Muehleman, *Acta Orthop.*, 2007, **78**, 536–546.
66. K. Potter, J. J. Butler, C. Adams, K. W. Fishbein, E. W. McFarland, W. E. Horton and R. G. Spencer, *Matrix Biol.*, 1998, **17**, 513–523.
67. J. B. Greco and R. G. Spencer, in *Bioreactors for Tissue Engineering: Principles, Design and Operation*, ed. J. Chaudhuri and M. Al-Rubeai, J Kluwer Academic Publishers, 2005.
68. F. De Ceuninck, C. Lesur, P. Pastoureau, A. Caliez and M. Sabatini, *Methods Mol. Med.*, 2004, **100**, 15–22.
69. Z. Yin, *Crit. Rev. Biomed. Eng.*, 2014, **42**, 137–191.
70. Z. Yin, T. M. Schmid, L. Madsen, M. Kotecha and R. L. Magin, Proceedings of the International Society for Magnetic Resonance in Medicine (ISMRM) 20th Annual Meeting and Exhibition, Melbourne, Australia, 2012.
71. G. Zernia and D. Huster, *NMR Biomed.*, 2006, **19**, 1010–1019.
72. D. Huster, G. Zernia, S. Hohle, R. Schulz, M. Zscharnack, J. Schiller, A. Bader and K. Arnold, *Biophys. J.*, 2005, **88**, 519a.
73. D. Huster, L. Naji, J. Schiller and K. Arnold, *Appl. Magn. Reson.*, 2004, **27**, 471–487.
74. D. Huster, J. Schiller and K. Arnold, *Magn. Reson. Med.*, 2002, **48**, 624–632.
75. W. Ling, R. R. Regatte, M. E. Schweitzer and A. Jerschow, *NMR Biomed.*, 2008, **21**, 289–295.
76. D. Huster, J. Schillar, L. Naji, J. Kaufmann and K. Arnold, *Lect. Notes Phys.*, 2004, **634**, 465–503.
77. M. Kotecha, T. M. Schmid and R. L. Magin, *presented in part at the Annual Meeting of the Biomedical Engineering Society Atlanta*, Georgia, 2012.
78. G. Navon, H. Shinar, U. Eliav and Y. Seo, *NMR Biomed.*, 2001, **14**, 112–132.
79. G. Jaccard, S. Wimperis and G. Bodenhausen, *J. Chem. Phys.*, 1986, **85**, 6282–6293.
80. G. Madelin and R. R. Regatte, *J. Magn. Reson. Imaging*, 2013, **38**, 511–529.
81. G. Madelin, J. S. Lee, R. R. Regatte and A. Jerschow, *Prog. Nucl. Magn. Reson. Spectrosc.*, 2014, **79**, 14–47.
82. A. J. Wheaton, A. Borthakur, E. M. Shapiro, R. R. Regatte, S. V. Akella, J. B. Kneeland and R. Reddy, *Radiology*, 2004, **231**, 900–905.
83. W. Ling, R. R. Regatte, G. Navon and A. Jerschow, *Proc. Natl. Acad. Sci.*, 2008, **105**, 2266–2270.